Military Technical College,
Kobry El-Kobbah,
Cairo, Egypt

9th International Conference
On Aerospace Sciences &
Aviation Technology

EXPERIMENTAL AND THEORETICAL INVESTIGATION OF VORTEX SHEDDING FROM SQUARE AND SHARP LEADING EDGE OF OSCILLATING FLAT PLATE.

by
Dr. Eng. Rasheed. A. Atta *

1- ABSTRACT

This paper investigates experimentally and numerically : the vortex shedding and dynamic stall for an oscillating flat plate with sharp and square leading edge at different angles of attack. Experiments showed a drastic and different flow pattern even if the flow is laminar. Flow visualization using hydrogen bubble technique yieldes an insight into not only in the vortex generation but also it showed a reverse flow and a unique succession of vortical development over the sharp leading-edge of the oscillating plate at different frequencies and amplitudes , even at a constant Strouhal number. Pressure field has been determined experimently.

A numerical solution for flow over a pitching flat plate on the basis of a finite difference analysis of the two-dimensional Navier-Stokes equations has been employed. Numerical computation confirms that vortex shedding from flat plate with square leading-edge is caused by the impinging shear layer instability, and provides some crucial information on the vortical flow occuring near the leading-edge in conjunction with the vortex shedding mechanism. Pressure field was determined too. Comparison between experimental and computational results has been considered.

2- KEY WORDS

VORTEX, LEADING-EDGE, UNSTEADY, VISUALIZATION, OSCILLATING PLATE.

3- NOMENCLATURE

f	The forcing frequency of the plate.
c	The plate chord.
U	The freestream flow velocity.
α	Mean angle of attack.
k	The reduced frequency= fc/U
$\Delta\alpha$	Amplitude of oscillation
t	Plate thickness
ω	vorticity
τ	shear stress

* Associate Prof./ Power and Energy Dept/ Faculty of Eng.,/ Minia Univ.,

4- INTRODUCTION

The unsteady flow structure from surfaces at high angle of attack ; supermaneuvers and flutter phenomena is of central importance in loading of helicopter blades undergoing transient motion, turbulent machinery blading, as well as wind turbine blades operating near optimum performance. In this cases, occurence of unsteady stall can substantially alter the lift if compared with the unstalled surfaces. Aerodynamic research of time-dependent viscous flows at high incidence of a two-dimensional surfaces have shed considerable light on the complex viscous- inviscid interactions associated with time-varying flow separation. The studies on the unsteady 2-D surfaces have indicated that the lift and drag experience hysteresis loops during an oscillation. It has been demonstrated that by properly executing post-stall maneuvers. During these maneuvers, there is typically a sudden increase in pitch up to the post-stall condition Herbst [1]. A further application of this class of flows involves a mean drag acting on the surface at high angle of attack. However in the event that a plate is inclined at an angle of attack other than 90°, the issue arises whether a reduction in mean drag can be accomplished by perturbing the plate such that the entrainment associated with small-scale vortex interaction changes the mean phase pressure and the shape of the separation surface from the leading- and trailing edges of the plate. The experimental work in the past showed that the flow field around an oscillating airfoil in subsonic flow can be characterized by the degree of extent of flow separation McCrosky et al [2,3]. The primary parameter that determines the degree of separation is the maximum angle of attack; the importance of the maximum angle of attack portrays two important regimes of viscous-inviscid interaction :

(i) very little separation occurs at certain values of maximum angle of attack although some viscous effects were noted.

(ii) When increasing the maximum angle of attack, a limited amount of separation occured during a small fraction of the cycle and distorted the hysteresis loops of the unsteady pressures and loads. From the practical point, the effect on the moment and drag coefficients are important.

A review of an oscillating flat plate may be summrized as follows : -

In the case where the plate is at zero and small incidence angle, the flow remains attached untill the trailing-edge, where vortices are shed harmony with the body motion . These shedding vortices and their counterparts that are bound around the surface, introduce a phase shift in fluid loading. A light stall may occur as a separation upstream of the trailing edge McCrosky [2,3].

The flow has been divided into two components : -

(i) Noncirculatory component of sources and sinks , which satisfies the boundary conditions of the oscillating plate, and which therefore includes the apparent masses.

(ii) Circulatory component which includes bound vortices and wake vortices and which is matched to the non-circulatory component at the trailing-edge in such a manner to enforce the Kutta condition of nonsingular flow there.

If the body or the flow fluctuates, so the pressure and circulation will change too, each change in circulation around spanwise is accompanied by shedding of vortex in the trailing-edge into the wake behind.

If the elastic axis (axis of rotation) is located at mid-chord, then there are no longer lift and moment components induced by pitching (torsional) and bending motions respectively. In order to complete the simulation of the plate oscillation in a real flow, it is necessary to account for the shedding of vortices from its trailing- edge (circulatory flow), in doing so, unsteady flow will leave the trailing-edge and the pressure will become finite.

Now for the practical case of an isolated plate oscillating in incompressible flow with its elastic axis aft of the mid-chord location, that will result on an energy transfer from the plate to the fluid. For a slender, rigid, unstalled surface, there will be no coupled-mode flutter if the center of gravity lies ahead of the elastic axis. If the plate is at sufficiently high incidence in subsonic flow, then there is a possibilty of flow separation, or dynamic stall, substantially altering the unsteady loading McCrosky et al [3]. Gad El-Hak and Ho [4] explained that the complex unsteady flow field associated with the pitching 2-D slender surfaces, can be explained by the mutual induction between the leading-edge vortex and the trailing-edge shedding vortex.

At large angle of attack, the flow separates at the leading-edge and a clockwise vortex is formed and is convected downstream. Ho & Huere [5] showed that the flow over the thin plate in dynamic oscillation represents two streams " most common laminar " of non-equal velocities moving on the upper and down surface are assumed to give rise, by viscous diffusion, to a weakly diverging steady basic flow of velocity field $U(x,y)$.

The development of mixing layers downstream of a slender plate is initially dominate by a linear instability mechanism Drazin & Howard [6]. The basic vorticity distribution which possesses a maximum, is inviscidly unstable to small perturbations. Thus two dimensional waves grow exponentially with downstream distance and are observed to roll up into vortices.

Beyond the region of exponential growth, Kelvin-Helmholtz instability waves evolve into a periodic array of compact vortices moving at the average velocity U. The sensitivity of shear layers to initial conditions is illustrated by Ho & Huang [7], who showed that the excitation becomes the first subharmonic of the initial vortex passage frequency, neighboring vortices are displaced and subsequently wrap around each other to form a single structure. From the previous study a vortex formed or separation occurs on the surface of a thin oscillating plate, in addition to the wake formed behind it will effect the drag, since the dynamic pressure in the wake will be reduced.

Stokes & Welsh [8] summarized the four regimes of vortex shedding obtained for flat plates with square leading and trailing-edges for various values of the chord-to- thickness ratio , the present work is applied for long plates chord-thickness ratio $c/t=20$ where the shear layers are always reattached upstream of the trailing-edges and form a separation bubble which grows, fluctuates in length and divides in a random manner. The vortices are randomly distributed and diffused before reaching the trailing edge. The experiments were devised to provide new insight into the influence of the motion time history on the dynamic stall and the resultant loading.

On the other hand computational fluid dynamics has made it possible to study the dynamic stall of oscillating flat plate numerically, by treating the full time- dependent Navier-Stokes equations Wu & Wang et al [9].

During the final stage of the upstroke and throughout the downstroke of the oscillation when flow separation becomes extensive, serious inaccuracies often become evident also in the computed aerodynamic lift and moment. In the present study of dynamic stall of oscillating surfaces relatively small and large amplitude motions (up to +10 °) for different mean angles of attack (from 0° to 90°) has been considered.

The experimental and computational results show that, under quiet general circumstances, deep stall flow fields are expected to contain several distinct flow components. There are vortical flow components where the vorticity field is not zero and the effects of viscous forces are important. These vortical components surround and trail the plate and are composed of a near vortical system and a trailing system. It is important, however, to recognize that the vortical system are surrounded by a large zone where the vorticity is essentially zero and the viscous force is, in consequence, negligible.

Also, within the vortical systems, two zones with distinct physical and mathematical characters co-exist. These two zones are designated attached and detached zones respectively. The attached zone contains the unsteady boundary layers. The most prominent features observed in deep stall experiments is the vortex structures which is a part of the detached vortical zone. Yuji et al [10] studied numerically the effect of chord to thickness of flat plate on the vortical flow field insabilitiy.

This study will shed light to avoid or reduce the undesirable effects as flutter, viberations, and dynamic stall through a proper understanding of the flow structure and its behaviour. Also it aims to establish a comprehensive understanding of the physical mechanisms associated with the generation of unsteady aerodynamic forces acting on lifting surfaces undergoing large amplitude unsteady motion . Also to identfy and characterize computationally the vortex structures produced through the study of the time-dependent flow over the flat plate, even for deep stalls .

5- EXPERIMENTAL TECHNIQUES and ARRANGEMENTS

Experiments has been done in an open water channel 25 *cm* x 20 *cm* crosssection with a 20 *cm* water depth. The Reynold number reached up to 15,000 based on the 50 *mm* plate chord with 2.5 *mm* thickness shown in figure 1-a, the plate is pivoted about the mid-chord. The forcing frequency has been done by a cam-d.c-motor system. The plate has been located at a mean angles of attack of 0°, 10° and 90° respectively and oscillates at two different amplitudes 3.5° and 10° . The working reduced freuency (k = fC/U) goes up to 9. An arrangment for pressure field measurements was done by making a 0.5 *mm* tapes at specified locations on both surfaces of the plate , these tapes were connecting to a digital micromanometer of accuracy (+ 0.05) *mm* of water, this micromanometer was mounted on a traverse mechanism with a displacement accuracy of (+ 0.1 *mm*).

Flow visualization has been done in the water channel using the hydrogen bubble technique with the straight and the zig-zag wire types. Flow visualizations were used to obtain time and position measurements for characteristic vortex development events. Temporal relationships between events could be calculated

6- MATHEMATICAL FORMULATION

The general strategy of the present study is to simulate in details the development of the vorticity field in the unsteady flow field surrounding a rapidly pitched plate through the numerical solution of appropiate flow equation. Simulation of the development of vorticity field therefore leads to correct predictions of the unsteady aerodynamic load. The physical processes of convection and diffusion alters the vorticity distribution in an unsteady flow. These processes are described by the well-known vorticity transport equation.

For two-dimenional incompressible laminar flow, the continuity and Navier-Stokes equations are :

$$\partial u/\partial x + \partial v/\partial y = 0 \quad (1)$$

$$\partial u/\partial t = - u\, \partial u/\partial x - v\, \partial u/\partial y - (1/\rho)\, \partial p/\partial x + \nu\, \partial^2 u/\partial x^2 + \nu\, \partial^2 u/\partial y^2 \quad (2)$$

$$\partial v/\partial t = - u\, \partial v/\partial x - v\, \partial v/\partial y - (1/\rho)\, \partial p/\partial y + \nu\, \partial^2 v/\partial x^2 + \nu\, \partial^2 v/\partial y^2 \quad (3)$$

where t is the time coordinate in an inertial reference frame moving at a velocity $-u_\infty$ relative to the freestream, u and v are respectively x- and y- velocity components, p is the pressure, ρ is the densty and ν is the kinematic viscosity of the fluid, taken to be constant for simplicity.

The vorticity ω is defined by :

$$\omega = \partial v/\partial x - \partial u/\partial y \quad (4)$$

Taking the x- and y- derivatives respectively of eqs. 3 and 2 and combining the results, one obtains after some manipulations the following vorticity transport equation

$$\partial \omega/\partial t = - u\, \partial \omega/\partial x - v\, \partial \omega/\partial y + \nu\, \partial^2 \omega/\partial x^2 + \nu\, \partial^2 \omega/\partial y^2 \quad (5)$$

The set of equations 1, 4 and 5 is equivalent to the set 1,2 and 3. Consider the use of the set 1, 4 and 5 in computing the development of the vorticity field with time . Equation 5 is a parabolic differential equation in its time-space relationship. This means that in solving this equation, it is possible to march forward in time. Begining with a known set of initial vorticity values at an old time level and solves equation. 5 to obtain a new set of vorticity values at a new time level, this new set of vorticity values is then used as initial values and eq. 5 is again solved to obtain vorticity values at a subsequent new time level. To implement this step-by-step procedure that advances the vorticity solution progressively in-time, one obviously needs to know the velocity distrbution at each time level because the convective process, represented by the first two terms on the right side of eq. 5, contribute to the transport of vorticity in the fluid. In addition, since eq. 5 contains an elliptic differential operator, i.e the Laplace operator, in space, the values of the vorticity on the boundary of the fluid region must be known at each time level to proceed with the computation.

For the present problem, the velocity boundary values are known at each time level from the prescribed motion. The vorticity boundary values are not specified directly by the physics of the problem and needs to be computed at each time level A computation loop which advances the vorticity solution from an old time level to a new time level composed of the following three major steps :

(1) Using known vorticity and velocity values at the old time level, new vorticity values at the interior of the fluid domain is computed for the new time level by solving eq. 5.

(2) New vorticity boundary values are computed.

(3) New velocity values at the new time level are computed.

Step (1) is concered with the kinetic processes that changes the vorticity distribution. Steps (2) and (3) are kinematic steps governed by eqs. 1 and 4 *i.e* is used to state the fact that eqs.1 and 4 express the relationship between the velocity field at any given instant of time and the vorticity fied at the same instant.

Equations 1, 4 and 5 are valid in all the three flow zones that co-exist in the overall unsteady flowfield. In the present study, these three equations are used only in computing the development of the vorticity field in the **detached** viscous zone.

For the flow Reynolds number of interest to the present study, certain simplifications are justifiable in the attached vortical zone. Using these simplifications, the set of equations 1, 2 and 3 reduces to the well-known boundary layer equations, and eqs 4 and 5 reduce to :

$$\omega = - \partial v_s / \partial n \qquad (6)$$

and

$$\partial\omega/\partial t = - v_s \, \partial\omega/\partial s - v_n \, \partial\omega/\partial n + \nu \, \partial^2\omega/\partial n^2 \qquad (7)$$

where s and n are the boundary layer coordinates tangential and normal to the plate surface respectively and v_s and v_n are respectively the s- and n-components of the velocity vector in the attached.

Equations 1, 6 and 7 describe the flow in the attached zone accurately. They are used in the present study to compute the development of the vorticity field in the attached zone.

In the potential flow zone, the vorticity and its gradient are everywhere zero. Since each term in eq. 5 is zero, there is no need to compute the development of the vorticity field with time in this zone.

It is recognized that, in a time-dependent flow, the processes of vorticity transport reshape the vortical zones as time progresses. A numerical method developed permit not only the evolution of the vortical zones to be followed computationally in such a way that only the vortical zones, and not the potential zone, need to be included in the solution procedure at each time level but also the two vortical zones to be sloved separately.

Equations 1 and 4 are re-expressible as integral representations for the velocity components :

$$u_{(x,y)} = - (1/2\pi) \int_R \int \left| (y - y_o) \, \omega_o / \, [(x - x_o)^2 + (y - y_o)^2] \right| \, dx_o \, dy_o + u_\infty \qquad (8)$$

and

$$v_{(x,y)} = (1/2\pi) \int_R \int \left| (x - x_o) \, \omega_o / \, [(x - x_o)^2 + (y - y_o)^2] \right| \, dx_o \, dy_o + v_\infty \qquad (9)$$

where R is the region occupied jointly by the fluid and the solid and ω_o is the vorticity at the point (x_o, y_o). In the solid region, ω_o is simply twice the angular velocity of the solid .

Equations 8 and 9 are valid for all three zones of the flow. In the attached zone, equations 1 and 6 gives the following integral relations that are comparatively simple :

$$v_{s\,(s,n)} = - \int_0^n \omega_{(s,n)} \, dn + v_{s\,(s,0)} \qquad (10)$$

$$v_{s\,(s,n)} = - \int_0^n \left[\partial v_{s\,(s,n)} / \partial s \right] dn + v_{n\,(s,0)} \qquad (11)$$

The pressure distribution $\partial p/\partial s$ and the shear stress on the surface of the plate are related to the value and the normal gradient of the vorticity on the surface by :

$$\partial p/\partial s = - \rho \nu (\partial \omega/\partial n) + \Omega (y_s . \partial x_s/\partial s - x_s . \partial y_s/\partial s) + \Omega^2 (x_s . \partial x_s/\partial s + y_s . \partial y_s/\partial s) \quad (12)$$

and

$$\tau = - \rho \nu \omega \quad (13)$$

where (x_s , y_s) give the instantaneous location of the point on the plate surface where $\partial p/\partial s$ is determined, Ω is the angular velocity of the plate and Ω is the angular acceleration. Equations 12 and 13 are used to evaluate the pressure distributions and the aerodynamic load in our work.

6-1 Removal of Potential Zone

Equation 1 states that a stream function ψ exists. Expressing u and v and derivatives of ψ and replacing the results into eq. 4, one obtains :

$$\partial^2\psi/\partial x^2 + \partial^2\psi/\partial y^2 = - \omega \quad (14)$$

The equations 1 and 4 are equivalent to eq. 14 and they constitute an elliptic system, the computation of velocity values, *i.e* step (3) of the computation loop discussed earlier, therefore represents a boundary value problem at each time step. The boundary of the flowfield is composed of an internal part and an external part .

The internal boundary is in contact with the plate surface. Velocity values on the internal boundary are known from the prescribed solid motion through the no-slip and the no-penetration conditions for a viscous flow. The external boundary is infinitely far from the plate surface. With a finite-difference method, the solution field is usually truncated. In the present study, the truncated region, however, is much smaller than those used in conventional numerical methods. The external boundary is located in the potential zone, but is not sufficiently far from the plate, and the velocity on this boundary differ substantially from the freestream velocity. Equations. 8 and 9 are used to compute the actual velocity values on the external boundary.

The removal of the potential zone from the computation procedure reduces drastically the number of grid points entering the computation procedure.

6-2 Vorticity Boundary Conditions

If the vorticity field ω is known in a connected region R and on the closed boundary B of this region, then the proper boundary condition for the kinematics of the present problem is expected to be either the normal velocity component v_n, which is equivalent to excepting an arbitrary constant, or the tangential velocity component v_s , which is equivalent to $\partial\psi/\partial n$, on B. In the present work both v_n and v_s on the plate surface are known from the physics of the problem.

Consider the case where ω is known in R and on B. If v_n is specified on B, then eqs 1 and 4 give a unique solution for the velocity field. This solution includes v_s values on the boundary B. If we specify the values of v_s on B, then in general these prescribed v_s values do not agree with the v_s values obtained as a part of the velocity field solution.

For the present problem, at any given time , ω is known in the interior of the region R from the kinetic part of the computation loop. In addition, v_n and v_s are both prescribed on B, therefore, ω is determined on Bas a result. In a problem where ω is in the known interior of the region R, then the specification on the boundary B of any two of the three variables v_s and v_n and ω determines the third variable on B.

Using the concept of that the values of ω on the plate can be computed accurately through the use of integral representations such as eqs 8 and 9 . For example, the discretization of eqs 8 and 9 yields a set of algebraic equations containing ω, u, v values at grid points in the interior of R and on B.

Since the vorticity boundary values are intimately related to pressure and the shear stress on the plate, as shown by eqs. 12 and 13, accurate determination of the aerodynamic load depends on accurate computations of the boundary vorticity values. In the present study, a Fourier series method is used in conunction with eqs. 8 and 9 to achieve superior computation efficiency in boundary vorticity computations.

6-3 Zonal Procedure

In figure 1-b are shown schematically the attached vortical zone, the detached vortical one and the potential one around the oscillating plate. As discussed earlier, the computation is confined to the two vortical ones, and they are carried out differently as follows :

For step (1) of the computation loop, eq. 7 is used in the attached one. Since the spatial differential operator in eq. 7 is parabolic, a marching procedure is used to advance the vorticity solution station by station downstream at each time level. The solution begines at the forward stagnation station and terminates at the demarcation line. In the present study, the demarcation line is placed significantly upstream of the separation point in order to avoid the improper use of the boundary layer simplifications in a part of the detached one. The needed boundary vorticity values for this part of the kinetic computation are on an open boundary composed of the forward stagnation station, a part of the plate surface and an external boundary. The vorticity values on the forward stagnation station are zero. The external boundary is placed in the potential zone where the vorticity values are zero. Vorticity values on the solid boundary are computed as discussed later.

Equation 5 is elliptic and is used in the detached one, an iterative procedure is used to obtain new vorticity values in the detached zone at each time level.

Boundary vorticity values are needed on a closed boundary composed of the demarcation lines, a part of the plate surface, the external boundary and a downstream boundary that cuts across the vortical wake. Vorticity values on the demarcation lines are obtained in the solution for the attached zone. Vorticity values on the external boundary are zero. Vorticity values on the plate surface are computed as discussed in the preceding section . This information will help to establish the total vorticity in the computation field at each time level .

The marching procedure for the attached zone is extremely efficient. In the present zonal procedure, the amount of computation needed for the attached zone is about 5% of the total amount.

The mostly iterative procedure is needed only in the detached zone. The number of grid points in the detached zone is drastically smaller than the total number of grid points required if all three zones, potential and vortical, are to be treated.

The attached zone is thin compared with the detached zone. With a non-zonal procedure, a single grid is usually used to accommodate both zones. Since the length scales of the two zones are very different, a large number of grid points is needed, particularly for high Reynolds number flows. The use of eq. 10 and 11 to compute velocity values in the attached zone is extremely efficient since only a one- dimensional array is involved at each station.

7- RESULTS and DISCUSSION

As a prelude to the study, the complex unsteady viscous flows on plates makes the problem attractive for exploring certain basic unsteady phenomena. The nonlinear effects of large amplitudes of oscillation and high reduced frequency increases the shear flows in such a way that it may change this trend towards flow reversal.

For the present experimental work, figure. 2 shows the oscillating plate at R_e= 6000 and at 0.0° mean angle of attack with an amplitude of +10°.
The left column of photos represents a low reduced frequency k= 0.5, it does not show vortex formation, but separation is clear. In the right set of photos, the reduced frequency is high and k = 6.0, the vortex generation from the leading edge is strong enough so that vortex may exist on both sides of the plate simultaneously. The generation mechanism of the vortex depends upon the forcing frequency. Comparing the flow structures over both the plate surfaces at the same angular positions during the up and down strokes, show clearly the phase shift between the plate position and vortex formation .

Figure. 3-a shows a close up views of a plate located at 10° mean angle of attack, oscillating with amplitudes of + 3.5°, the photos are compared at two similar plate instantaneous positions : at far up and far down positions indicates every small detail for two reduced specified frequencies (k= 0.6 and 2.0). The comparison shows formation and development of vortex at the leading-edge.

On the hand figure 3-b shows a complete cycle of vortex formation on the leading-edge of the plate located at a 10° mean angle of attack, at a reduced frequency k=2.0 : photo A is for the very high plate up position indicating the generation of a small vortex, while a previous vortex has been already amplified as it moves downstream. In photo B the tip reached in its downstroke the position where α=-10°, the small vortex in photo A which just started moved fast downstream simultaneously another new vortex is just born.

While in photo C a third vortex could be seen. It may be noticed that during one cycle we may count a three vortices at a reduced frequency = 2.0.

In figure. 4 as the angle of attack increases a deep stall region will occur and the separation zone becomes larger. The most severe condition will be reached when the plate is mounted at 90° with the flow motion similar to the supermanuver of aircraft.

As the sharp-edged plate oscillates around the 90°, R_e= 6000 and an amplitude of 3.5° , a set of vortex structure with a distinguished patterns were observed.

The left column of photos represent the flow structure where the plate edge is at the far left position, at different reduced frequencies, while the right column of photos represents the vortex structure on the plate edge at far right position at the same frequencies. The variation of the width of the wake region, type of vortex generated and development are clear in each set of photos.

In figure. 5 similar to figure. 4 except that the amplitude has been incresed to 10° instead of 3.5°, which indicates that the energy transfered to the fluid increases as well , but the periodic time of motion decreases rapidly. Consequently, the vortices sheded start to be subdivided in small ones and/or tend to spread away or the separation may result in a multiple or in a well organized pair of vortices.

The present computational work; the dynamic stall of a rapidly pitched flat plate is examined computationally.

The plate initially placed in a uniform flow at a zero angle of attack. After steady state results are obtained for this zero angle of attack position. The plate is set to rotate. The pitching rate α of the plate is kept constant until a maximum incident angle α_{max} is reached. The plate is then kept in this maximum incidence angle for an additional period of time.

The following are selected results of the present computed study , the computed results are compared with the experimental results done herein through pressure measurements. The deviations sometimes are significantly between experimental results and computational ones as for the assumptions made in the solution.

Figure. 6 represents the typical historical record of pressure shapes at four stages a, b, c and d. At (a), a pressure distribution similar in shape to those observed for steady unstalled airfoil. A suction peak exists in the leading edge region on the plate's upper surface. This stage persists beyond the static stall incidence angle.

At (b), the suction peak breaks away from the leading-edge region and moves downstream on the upper surfce of the plate. At (c), the pressure peak continues to move downstream. The magnitude of the peak decreases and the peak broadens over the plate in the stage. At (d), the pressure distributions flatten on both the upper and the lower surfaces. The pressure coefficients C_P on these two surfaces attain levels of nearly minus and plus unity respectively.

In figure. 7 are shown four sets of pressure distributions corresponding to the four stages of dynamic stall development α= 16°, 22° , 30° and 60°. The results shown in figure. 7 are for the flow and motion parameters of $R_e = 1.5 \times 10^4$, α_{max} = 60° and k = 0.2 . In stages (b) and (c) the computed pressure distributions contain minor spatial oscillations, which are absent in the experimental data, along the upper surface of the plate. The computed suction mgnitudes in stages (a), (b) and (c) are somewhat higher than the experimental values. The computed pressure distribution deviates a little from that measure shap in stage (d). In view of the assumptions made in the present computations, and of the experimental and measuring errors. We may suggest that the shapes of the pressure distributions are related to the forming and development of a strong dynamic stall vortex. In stage (a), the dynamic stall vortex is not yet formed and the vortical region of the flow contains in essence only the attached zone.

The dynamic stall vortex is formed and energized during stage (b). During stage (c), the vortex losses energy .During stage (d), the flowfield relaxes as if it about a bluff body.

In figure. 8 are shown computed streamlines (left and right columns) at incident angles corresponding to the pressure distributions in figure. 7. The streamlines clearly exhibit the forming, development and movement of a strong leading edge vortex during stages (b), (c) and (d), and also show the presence of secondary vortices on the upper surface of the plate. It is understandable that these secondary vortices are responsible for the minor-spatial oscillations observed in the pressure distributions of stages (b) and (c). During (a), the pressure distribution on the upper surface between x/c = 0.6 and x/c= 0.95 is nearly flat, as shown in figure. 7(a).

In the left column of figure. 8 are shown streamlines computed for $R_e = 1.5 \times 10^4$ and $k = 0.2$ at several successive time levels after the onset of the pitching motion of the plate.

The four stages of development of the dynamic stall flowfield are again demonstrated by these streamlines. In stage (a), a significant degree of trailing-edge separation is again present. In stages b, c and d, secondary vortices are present together with the strong leading edge vortex.

The left column of figure. 8 involves flow and motion paramters identical to those in he left column, except the Reynolds number is 2000 instead of 15,000. This reduced Reynolds number means a higher rate of momentum transfer across the shear layer, or the attached viscous zone. Although this momentum transfer is due to molecular viscosity, it is similar to flow turbulence in that it tends to retard flow separation.

A comparison of streamlines shown in both columns in figure. 8, for the higher Reynolds number case show that, the increased viscous diffusion effects suppress the formation of the secondary vortices.

8- CONCLUSIONS:

(1) For an oscillating flat plate, a separation , light and deep stall which showed different vortex patterns were found to be sensitive to the Reynolds number, reduced frequencies , the oscillation amplitude and the maximum angle of attack.

(2) Hysteresis is well noticable during a cycle , which effects the lift, drag and moment loading values.

(3) Higher Reynold number vortex flow, causes an increasing in viscous diffusion effects which suppress the formation of the secondary vortices .

(4) The generally good agreement between computed and experimental aerodynamic loads supports the view that computational predications of unsteady aerodynamics of rapidly pitched plates are feasible.

(5) For engineering design applications the ultimate goal of computational fluid dynamics is to be able to simulate three-dimensional high Reynolds number unsteady flows routinely.

(6) The physical features in unsteady stalled flowfields can be efficiently simulated and solved computationally.

9- ACKNOWLEDGEMENT

I'ld like to thank Prof. Wu (U.S.A) for his sincere co-operation in producing the computational part of this analysis, which gave support to the present work.

10- REFERENCES

1-Herbst, W. B.," Supermaneuverability in Unsteady Separated Flow" eds. M. S. Francis & M. W. Luttges, Univ. Colorado, p. 1, 1983.
2- McCrosky, W. J.," Unsteady Airfoils." Ann. Rev. Fluid Mech. 14, p. 285, 1982.
3-McCrosky, W. J., McAlister K. W., and Carr, L W.," Dynamic Stall Experiments on Oscillating Airfoils."AIAA J., Vol. 14, No. I, 1976, pp. 57-63.
4-Gad-El-Hak, M., Ho, C. M.," Three-Dimensional Effects on Pitching Lifting Surface" AIAA 23rd Aerospace Science Meeting, Jan 14-17, 1985/ Reno, Nevada.
5-Ho, C. M., Huerre, P., " Pertubed Free Shear Layers, " Ann. Rev. Fluid MECH. 1984 , V. 16, p 365.
6-Drazin, P. G., Howard, L. N.," Hydrodynamic Stability of Parallel Flow of Inviscid Fluid " Adv. Appl. Mech. V. 9 . pp 1, 1966.
7-Ho, C. M., Huang, L. S., " Subharmonics and Vortex Merging in Mixig Layers." J. Fluid Mech. V. 119, pp 443-473, 1982.
8-Stokes, A. N., & Welsh, M.C . " Flow-Resonant Sound Interaction in a Duct Containing a Plate, II : Square Leading edge. J. Sound Vib. 104, 55-73, 1996.
9-Wu, J.C., Wang, C.M., Wu, Jiunn-Chi and Sankar, N.L., " Dynamic Stall of Oscillating Airfoils," Proceedings of AHS 22nd Forum, American Helicopter Society,1986.
10-Yuji O., Yasuharu N., Shigehira O., Hideki T., and Ryuzo N.," A Numerical Study of Vortex Shedding from Flat Plates with Square Leading and Trailing Edges" J. Fluid Mech. Vol. 236. pp 445-460. 1992.

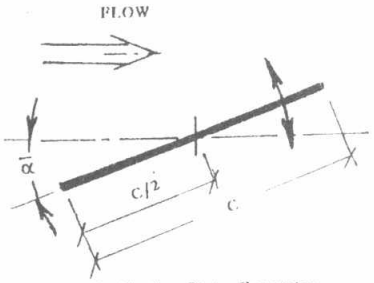

Fig. 1-a Oscillating Plate Geometry

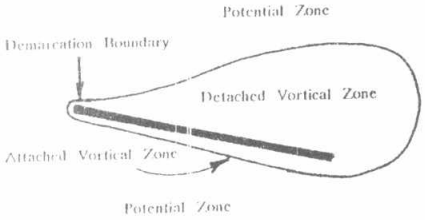

Fig. 1-b Computation Zones & Boundaries

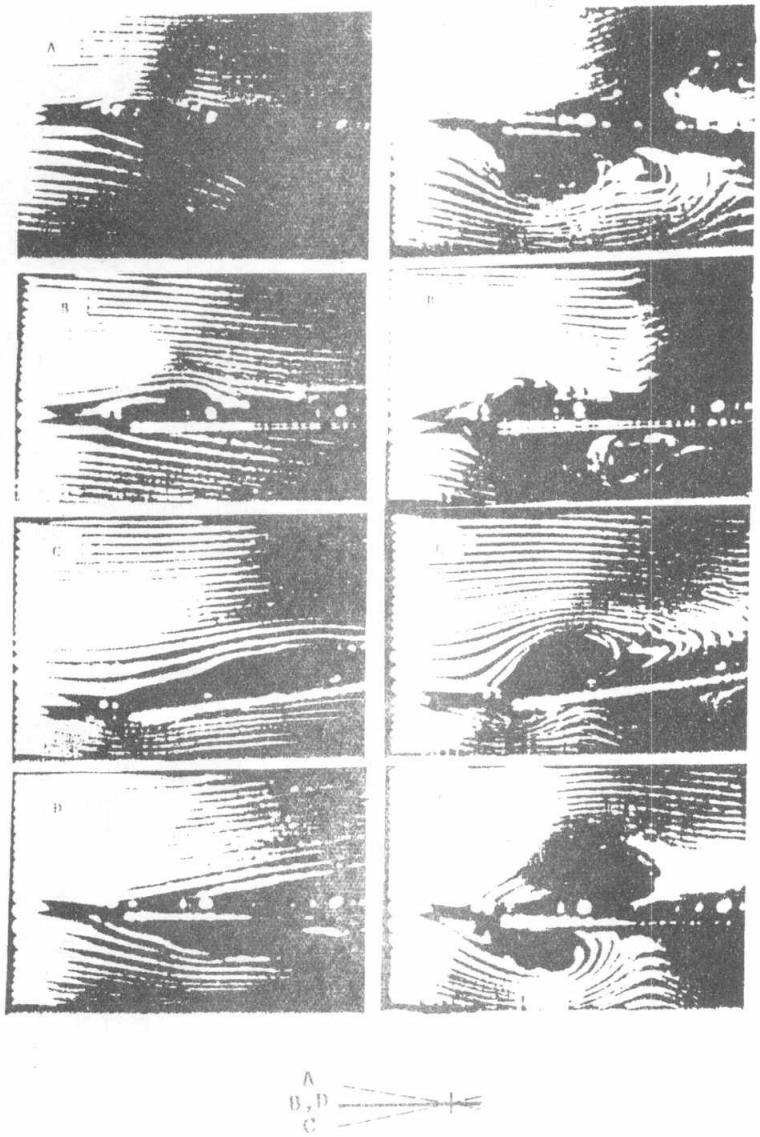

Fig.2 A comparison of time sequence of flow structure during one cycle of plate motion at k= 0.5 (left) and k= 6.0 (right), $\alpha = 0^{o}$, $\Delta\alpha = 10^{o}$

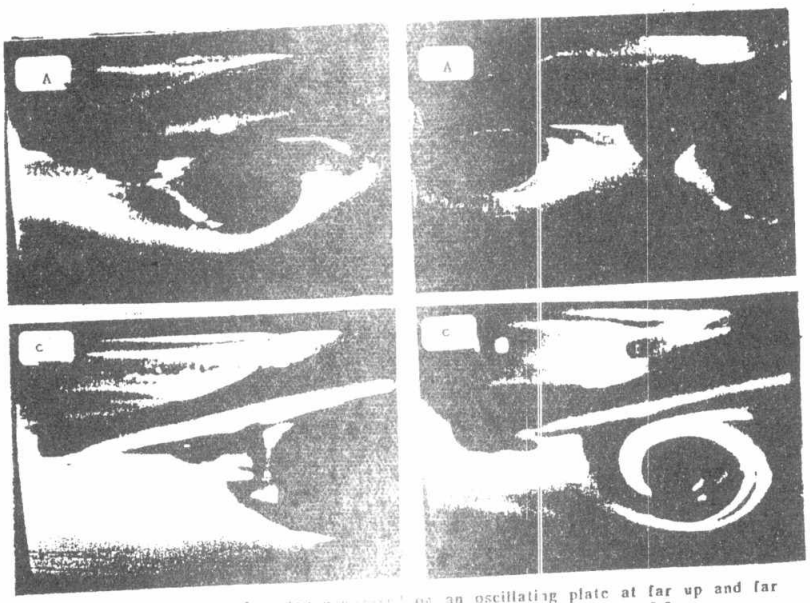

Fig.3-a Close up view of vortex generation on an oscillating plate at far up and far down plate positions; $\alpha = 0^{\circ}$, $\Delta\alpha = 3.5^{\circ}$ for k = 0.6 and k = 2.0 .

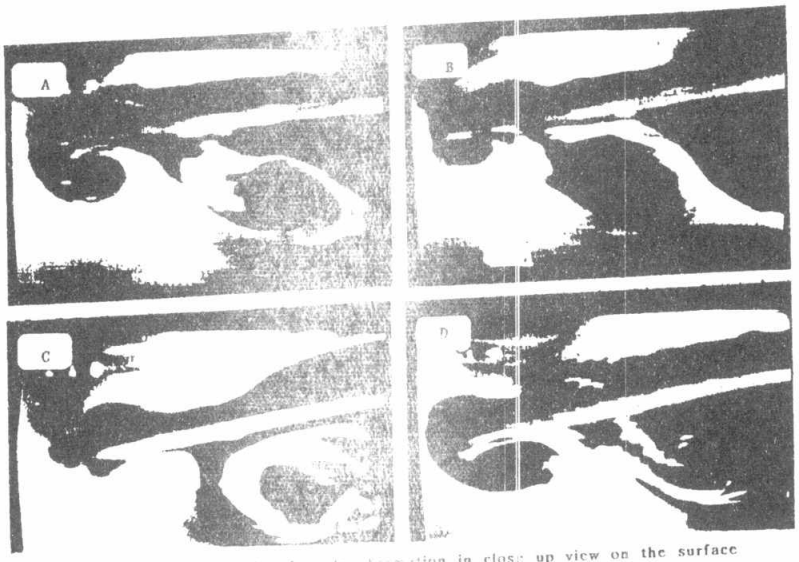

Fig.3-b A complete cycle of vortex formation in close up view on the surface of oscillating plate $\alpha = 0^{\circ}$, $\Delta\alpha = 3.5^{\circ}$ at k = 2.0

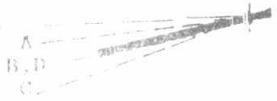

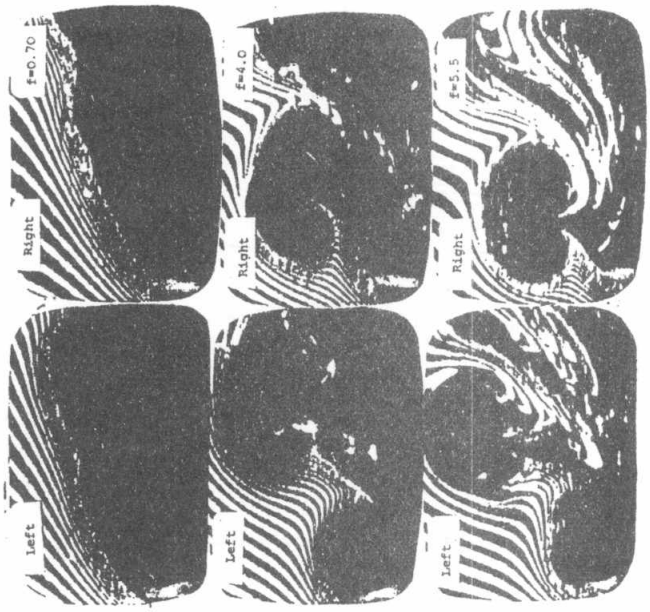

Fig.5 Flow structure shed from a 90^{o} sharp L.E of flat plate, $\Delta\alpha = 10^{o}$, $Re = 6000$, at far positions.

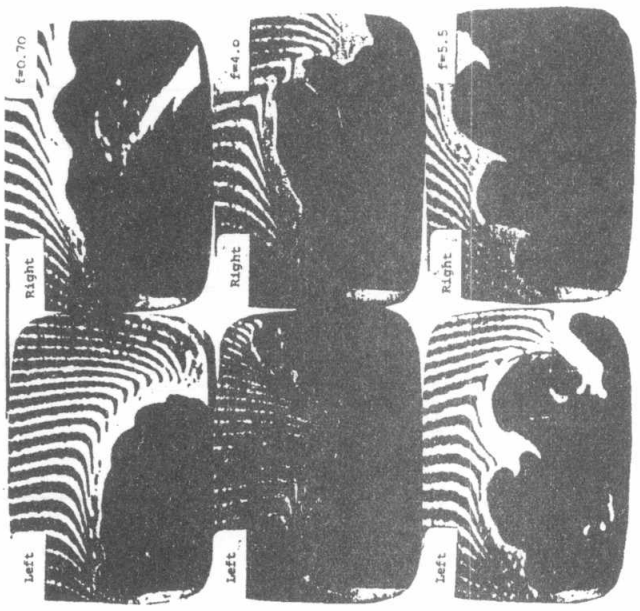

Fig.4 Flow structure shed from a 90^{o} sharp L.E of flat plate, $\Delta\alpha = 3.5^{o}$, $Re = 6000$, at far positions.

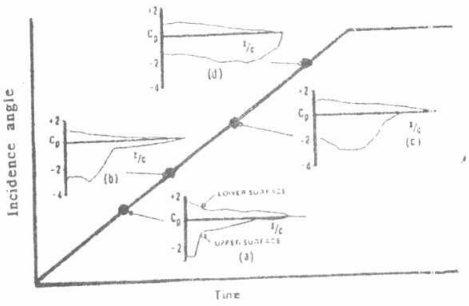

Fig.6 Typical correlation between pressure distribution and pitch motion time history.

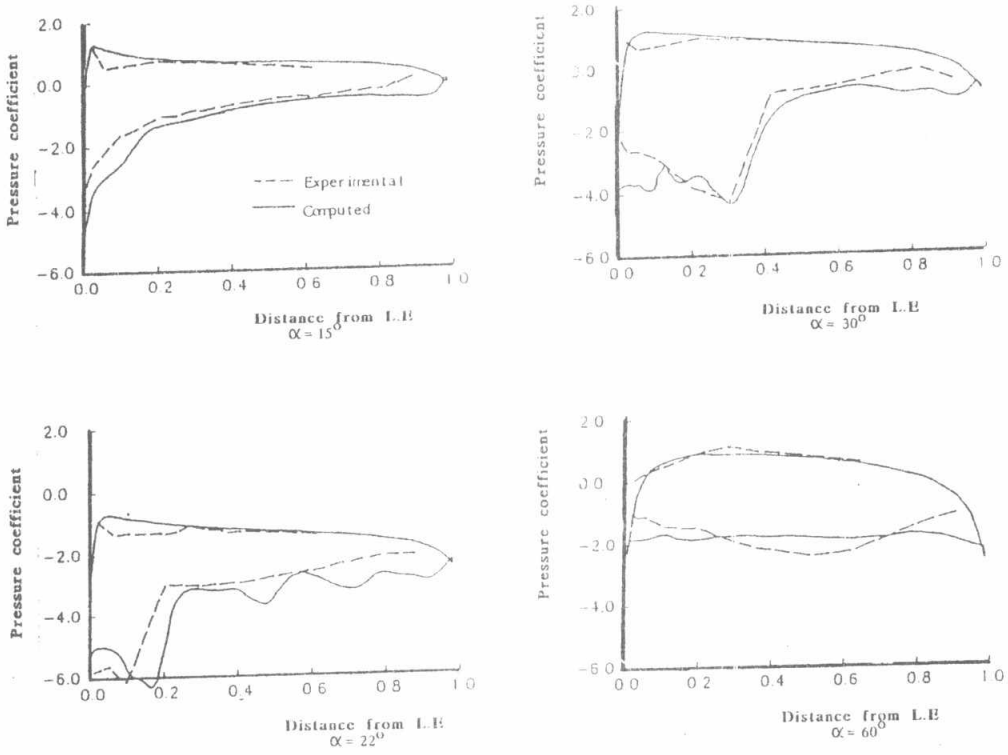

Fig.7 Pressure distribution of a pitched flat plate $Re = 1.5 \times 10^4$ and $k = 0.2$.

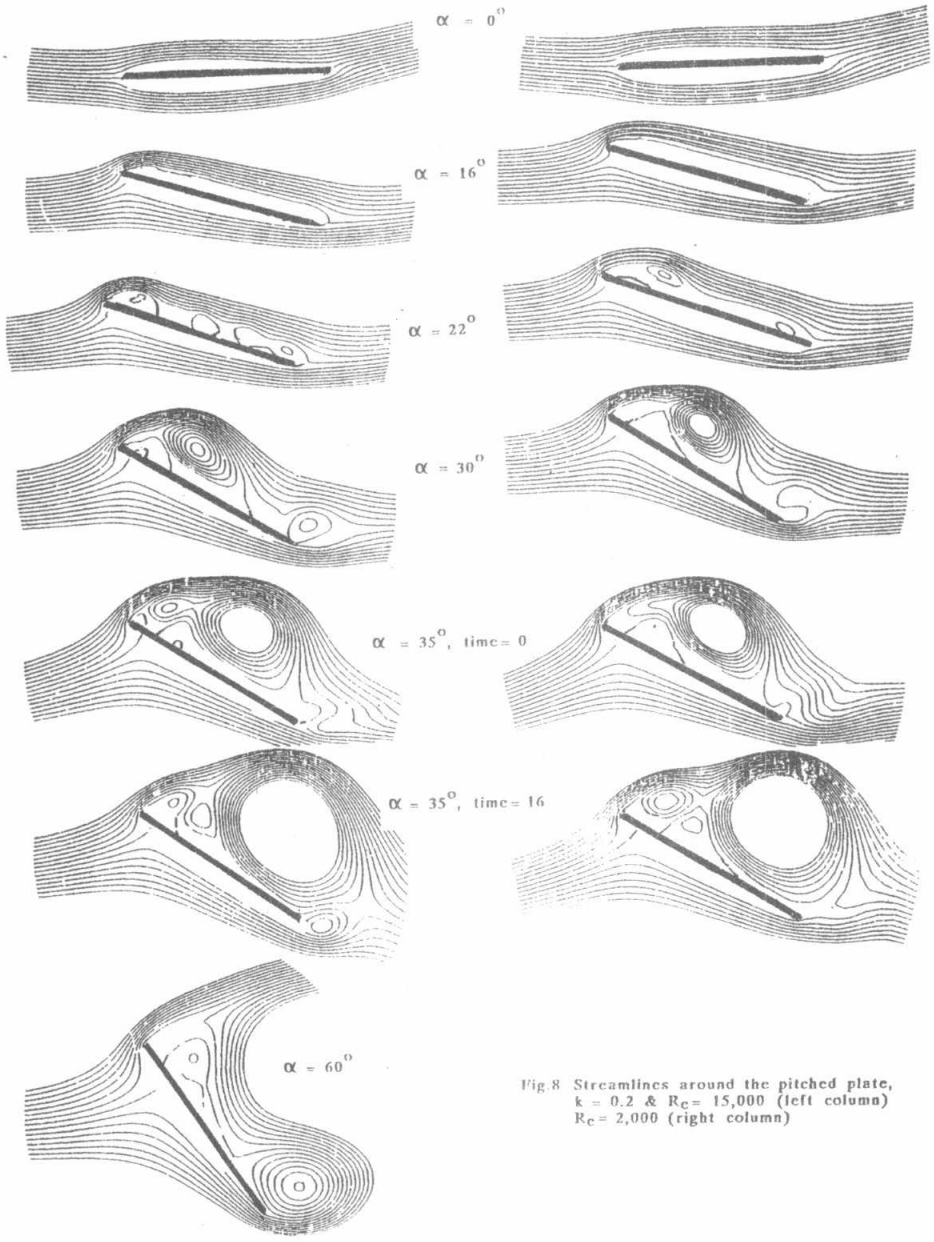

Fig.8 Streamlines around the pitched plate, k = 0.2 & R_e = 15,000 (left column) R_e = 2,000 (right column)